EDGE ARTICLE

Flexible organic frameworks sequester neuromuscular blocking agents *in vitro* and reverse neuromuscular block *in vivo*†

Yan Wu, [a] Yue-Yang Liu, [a] Hong-Kun Liu,[a] Shang-Bo Yu, [b] Furong Lin, [b] Wei Zhou, *[a] Hui Wang,[a] Dan-Wei Zhang, *[a] Zhan-Ting Li *[a] and Da Ma *[c]

Supramolecular sequestration and reversal of neuromuscular block (NMB) have great clinical applications. Water-soluble flexible organic frameworks (FOFs) cross-linked by disulfide bonds are designed and prepared. Different linker lengths are introduced to FOFs to give them varied pore sizes. FOFs are anionic nanoscale polymers and capable of encapsulating cationic neuromuscular blocking agents (NMBAs), including rocuronium (**Roc**), vecuronium (**Vec**), pancuronium (**Panc**) and cisatracurium (**Cis**). A host–guest study confirms that FOFs bind NMBAs in water. The multivalency interaction between FOFs and NMBAs is able to sequester NMBAs, and prevent them from escaping. These FOFs are non-toxic and biocompatible. Animal studies show that FOFs are effective for the reversal of NMB induced by **Roc**, **Vec** and **Cis**, which shorten the time to a train-of-four ratio of 0.9 by 2.6, 3.8 and 5.7-fold compared to a placebo, respectively.

Introduction

The sequestration of pharmaceutical agents, drugs and toxins has great clinical applications.[1–3] The clinical uses of sequestration include emergency treatments for drugs of abuse,[4–6] the prevention of harmful side effects of pharmaceuticals,[7,8] or the reversal of neuromuscular block (NMB).[9–11]

Supramolecular sequestration often serves as a pharmacokinetic approach, and involves molecular recognition.[12–14] One important clinical example of a supramolecular sequestration agent is sugammadex, a γ-cyclodextrin derivative, which binds neuromuscular blocking agents (NMBAs) and reverses their NMB.[15–17] Other molecular containers, including cucurbit[*n*]uril-family hosts and water-soluble pillar[*n*]arenes have also been reported to sequester NMBAs.[18–21] Nevertheless, molecular containers lack the structural tunability to be optimized for the binding of NMBAs and other sequestration targets. By contrast, framework materials may be fine-tuned for binding and

sequestration by simply changing the building blocks and cross-linkers.[22,23]

Herein, we explore the sequestration of NMBAs by framework materials. Metal–organic frameworks (MOFs),[24–26] covalent–organic frameworks (COFs)[27,28] and supramolecular–organic frameworks (SOFs)[29–31] are important framework materials. To sequester NMBAs, we use a new type of framework, flexible organic frameworks (FOFs), which are biocompatible, stable and capable of encapsulating pharmaceutical or biological guests.[32–34] For this purpose, FOFs cross-linked by disulfide bonds are prepared and used. The resulting water-soluble anionic FOFs are capable of encapsulating NMBAs through hydrophobic and electrostatic interactions. Considering the original intention of modular design, different core moieties were introduced which realized the change in pore size of FOFs and the size of hydrophobic surfaces. These FOFs are confirmed to effectively sequester NMBAs *in vitro* and reverse the NMB *in vivo*.

Results and discussion

Synthesis of precursors T1–T3

The synthetic routes of precursors **T1–T3** are outlined in Schemes S1–S3,† respectively. The linker moiety Boc-Cys(Trt)-Asp-(OMe)$_2$ was synthesized from two essential amino acid derivatives by the conventional EDCI/HOBt condensation reaction. Triphenylmethane is a sulfhydryl protective group sensitive to medium-strong acid. Formic acid was used to remove the Boc protecting group to yield Cys(Trt)-Asp-(OMe)$_2$. The EDCI/HOBt condensation reaction failed to achieve high yield

[a]Department of Chemistry, Shanghai Key Laboratory of Molecular Catalysis and Innovative Materials, Fudan University, Shanghai 200438, China. E-mail: zhouw@fudan.edu.cn; zhangdw@fudan.edu.cn; ztli@fudan.edu.cn

[b]Key Laboratory of Synthetic and Self-Assembly Chemistry for Organic Functional Molecules, Shanghai Institute of Organic Chemistry (SIOC), Chinese Academy of Sciences, 345 Lingling Lu, Shanghai 200032, China

[c]School of Pharmaceutical and Materials Engineering & Institute for Advanced Studies, Taizhou University, 1139 Shifu Avenue, Jiaojiang, Zhejiang 318000, China. E-mail: dama@fudan.edu.cn

† Electronic supplementary information (ESI) available. See https://doi.org/10.1039/d2sc02456j

conversion in the next amidation step. Therefore, TCPM was converted to acyl chloride, followed by the reaction with amine. T1-(Trt)$_4$-(OMe)$_8$ was obtained in high yield by column chromatography and recrystallization (yield 56%). The protective group of sulfhydryl was removed by TFA. To protect the sulfhydryl group from oxidation in air, the Schlenk technique was used to maintain an anaerobic environment during the ester hydrolysis reaction to obtain **T1**. Detailed synthetic procedures are available in the ESI.†

For precursors **T2** and **T3**, acrylate and benzoate fragments were introduced into core moieties through the common coupling reaction, and then the modified derivatives of core moieties were obtained through ester hydrolysis.[35,36] The following module splicing, deprotection and ester hydrolysis reactions were operated using the procedures described for **T1**.

Construction and characterization of FOFs

As shown in Scheme 1, compounds **T1-3** were used as precursors to prepare **FOF-SS1-3**. Precursors **T1-3** shared the same core moiety of tetraphenylmethane and flexible linkers of cysteine–aspartic acid dipeptide, which were conjugated with a C–C single bond, ethylene group or *p*-phenyl group. The three different conjugation groups gave **FOF-SS1-3** different pore sizes and recognition cavities. The porous polymeric FOFs were constructed by dynamic covalent disulfide cross-linking with H$_2$O$_2$ oxidation under alkaline conditions. The resulting FOFs are three-dimensional porous structures based on precursors **T1-3** and cross-linked by disulfide bonds. Two monocationic NMBAs (rocuronium or **Roc** and vecuronium or **Vec**) and two dicationic NMBAs (cisatracurium or **Cis** and pancuronium or **Panc**) were chosen for the study.

We used ^{1}H NMR spectroscopy to study the formation of **FOF-SS1-3**. Briefly, precursors **T1-3** (5 mM) were dispersed in D$_2$O. Precursors were neutralized with a stoichiometric amount
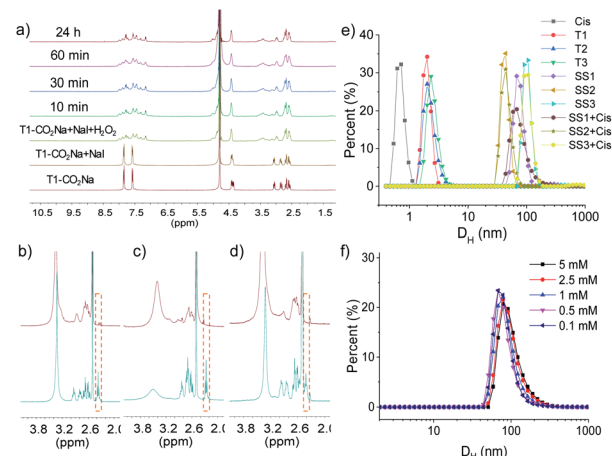

Fig. 1 (a) ^{1}H NMR spectra (400 MHz, D$_2$O, 298 K) recorded for the formation of **FOF-SS1** after the oxidant was added. ^{1}H NMR spectra (400 MHz, DMSO-d_6, 298 K) recorded for (b) **T1** and acidulated **FOF-SS1**, (c) **T2** and acidulated **FOF-SS2**, and (d) **T3** and acidulated **FOF-SS3**. (e) Size distribution of **Cis**, **T1-3**, **FOF-SS1-3** and **FOF-SS1-3** + **Cis** in water. (f) Size distribution of **FOF-SS1** at different concentrations in water (calculated based on [**T1**]).

of NaOH and oxidized by four equivalents of H$_2$O$_2$. Sodium iodide played a role as a catalyst in the oxidation process. This condition could ensure a rapid and clean oxidation reaction.[37] ^{1}H NMR spectra showed the emergence of a new set of resonances shortly after the oxidant was added, which remained unchanged after that (Fig. 1a, S10 and S11†). This observation indicated that the cross-linking reaction was rapidly completed. The originally sharp and clearly split peaks became wider and more complex, which proved the formation of a new material. After incubation for 24 h at 310 K, the ^{1}H NMR spectra remained the same as the initial state, confirming that an equilibrium had
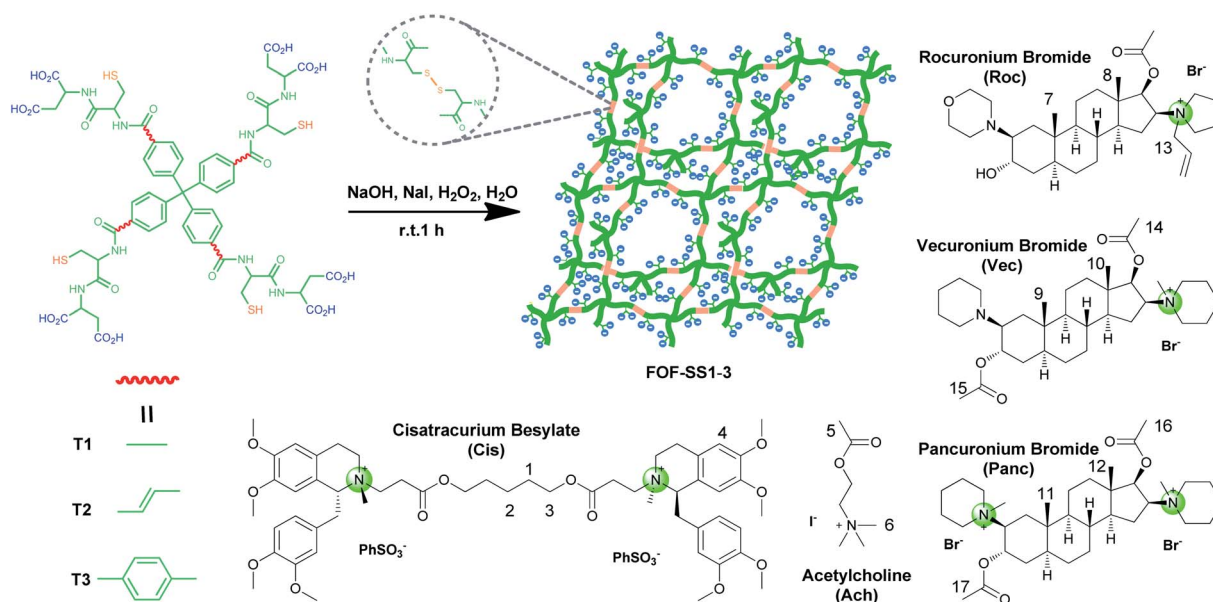
Scheme 1 Synthetic scheme for **FOF-SS1-3** and chemical structures of NMBAs and acetylcholine.

been quickly reached. To confirm the formation of disulfide bonds, the products of the **FOF-SS1-3** cross-linking reaction were acidulated by an excess amount of hydrochloric acid, and the precipitate was collected and dried under high vacuum. As shown in Fig. 1b–d, the proton resonance of sulfhydryl groups almost completely disappeared on the ^{1}H NMR spectra of acidulated **FOF-SS1-3**, which indicated the cross-linking of sulfhydryl groups and the formation of disulfide bonds.

Next, the formation of FOFs was investigated by dynamic light scattering (DLS) in water. Briefly, neutralized precursors **T1-3** (1 mM) were incubated in an aqueous solution of H_2O_2 (4 mM), and the size distribution was monitored by DLS. As shown in Fig. 1e, before H_2O_2 was added, precursors **T1-3** alone demonstrated a hydrodynamic diameter (D_H) of 2.0–2.3 nm. After incubation for one hour, the D_H of the reaction solution increased to 68 nm, 44 nm and 106 nm for precursors **T1-3**, respectively, confirming the cross-linking and formation of **FOF-SS1-3**. When **FOF-SS1-3** were diluted by 50 times, the hydrodynamic diameter did not show a noticeable change, suggesting that the cross-linking of FOFs prevented them from dissolution or swelling (Fig. 1f and S15†). Combined with the above stability test in ^{1}H NMR, the rapid formation and stability of the compound were verified which ensured repeatability of material preparation. When equivalent **Cis** was added, the hydrodynamic diameter of FOFs did not show a noticeable change, indicating that guest molecules did not have a significant impact on the size of FOFs. The size distribution of **Cis** (<1 nm) was not observed, which indicated that **Cis** was drilled into the cavities of FOFs rather than dispersed in the solution. All three FOFs were easily dispersed to form homogeneous and clear solutions in water up to 50 mg mL^{-1} due to the solubility enhancement of carboxylic acid groups. The carboxylic acid-rich structure also explained the negatively charged ζ potential, with that of −44.2 mV, −44.9 mV and −42.8 mV for **FOF-SS1-3**, respectively.

Supramolecular interaction between FOFs and NMBAs *in vitro*

The pore sizes of **FOF-SS1-3** were calculated to be approximately 3.0–4.9 nm, spacious enough to accommodate NMBAs. FOFs are abundant with negatively-charged carboxylic acid groups, which render them capable of binding cationic NMBAs. We used ^{1}H NMR spectroscopy to study the binding in water. As shown in Fig. 2a–c, when mixed with **FOF-SS3**, methylene protons (H$_1$–H$_3$) of the alkyl chains and the aromatic proton (H$_4$) in **Cis** underwent significant (0.25–0.3 ppm) upfield shifts.[38] In addition, other protons also moved upfield slightly, which suggested the shielding nature of FOF cavities. The same upfield shifted resonances were observed for **Cis** when mixed with FOF-SS1-2 (Fig. S16 and S17†). Similarly, when FOF-SS3 and steroidal NMBAs (**Roc**, **Vec** and **Panc**) were mixed, resonances of steroidal protons (H$_7$–H$_{12}$) shifted dramatically upfield (Fig. S18–S20†).[18] Therefore, FOFs are capable of encapsulating NMBAs.

A fluorescence titration experiment was employed to study the interaction between **Cis** and FOFs. Fig. 3a shows that with the gradual addition of **Cis** into a solution of **FOF-SS3** with a fixed concentration, the emission intensity at 752 nm decreased significantly. The emission intensity-**Cis** concentration curve reached a plateau when the concentration
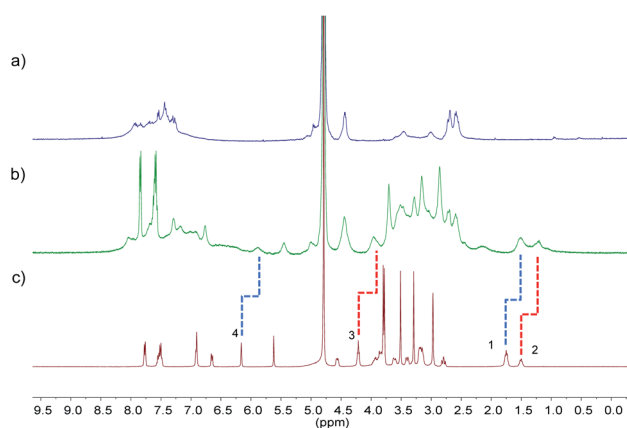
Fig. 2 ^{1}H NMR spectra (400 MHz, D$_2$O, 298 K) recorded for (a) **FOF-SS3** (2 mM, calculated based on [T3]), (b) a mixture of **FOF-SS3** (2 mM) and **Cis** (2 mM), and (c) **Cis** (2 mM).
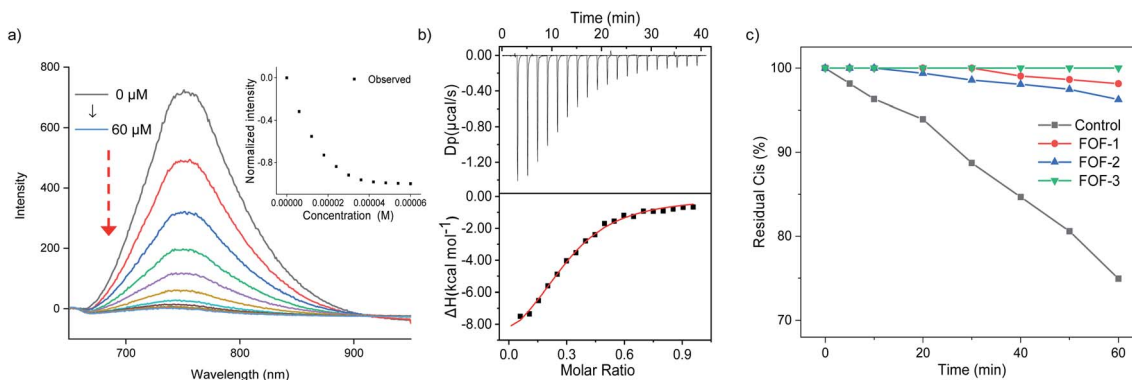
Fig. 3 (a) Fluorescence titration of **FOF-SS3** (50 μM in PBS) by adding **Cis** (0–60 μM), λ_{ex} = 325 nm and λ_{em} = 752 nm. (b) Plot of differential power (μcal s^{-1}) *vs.* time from the titration of **FOF-SS3** (0.1 mM) and with **Cis** (0.8 mM) in PBS (pH 7.4) and plot of the ΔH *vs.* molar ratio. The red line represents the best non-linear fit of the data K_a = (1.04 ± 0.11) × 10^5 M^{-1}. (c) The time-dependent change of residual **Cis** with FOFs in a dialysis bag. [FOF-SS1] = [FOF-SS2] = [FOF-SS3] = 10 mg mL^{-1} and [**Cis**] = 1 mg mL^{-1}.

Table 1 Binding constants (K_a, M^{-1}) for the complex of FOFs and NMBAs determined by ITC. Conditions: PBS, pH 7.4, 298 K

NMBAs	FOF-SS1	FOF-SS2	FOF-SS3
Cis	$(1.56 \pm 0.65) \times 10^4$	$(3.11 \pm 0.41) \times 10^4$	$(1.04 \pm 0.11) \times 10^5$
Roc	$(1.39 \pm 0.86) \times 10^4$	$(1.30 \pm 0.37) \times 10^4$	$(2.78 \pm 0.50) \times 10^4$
Vec	$(1.33 \pm 0.47) \times 10^4$	$(1.79 \pm 0.25) \times 10^4$	$(5.36 \pm 0.41) \times 10^4$
Panc	$(2.56 \pm 1.16) \times 10^4$	$(1.84 \pm 0.69) \times 10^4$	$(6.95 \pm 0.52) \times 10^4$

approached 50 μM. This observation indicated that **Cis** entered the cavity of the FOF and greatly reduced the fluorescence emission intensity, which could be explained by the electrostatic interaction between **FOF-SS3** and **Cis**.

To quantitatively analyze the binding strength, isothermal titration calorimetry (ITC) was employed to determine the binding constants of FOFs and NMBAs. The titration curves were well fitted with a 1 : 1 binding model. As shown in Fig. 3b, S21–S23.† The value of K_a for the complex of **FOF-SS1-3** and **Cis** was determined to be $(1.56 \pm 0.65) \times 10^4$ M^{-1}, $(3.11 \pm 0.41) \times 10^4$ M^{-1} and $(1.04 \pm 0.11) \times 10^5$ M^{-1}, respectively. The values of K_a for the complexes of FOFs and other NMBAs were determined by ITC and are summarized in Table 1. The binding strength between FOFs and all the four NMBAs was comparable, indicating that the electrostatic interaction between anionic carboxylate and cationic NMBAs was the key factor in determining the binding strength. The binding strength of **FOF-SS3** towards NMBAs was slightly higher compared to that of the other two FOFs, showing that the introduction of a benzene moiety into the FOF helped enhance hydrophobicity and improve binding strength. Acetylcholine (**ACh**) is a neurotransmitter involved in the NMB process. ^{1}H NMR spectroscopy was employed to compare the interactions between FOFs and **Ach** or **Cis** (Fig. S24†). When equivalent stoichiometric FOFs and **Ach** were mixed, significant (0.26–0.30 ppm) upfield shifts of H_5 and H_6 in **Ach** were observed. However, as **Cis** was added, even excessive **ACh** did not show stronger competitiveness. The signal of **ACh** was consistent with that of pure **Ach**, while that of **Cis** still moved upfield. The competitive assays showed that the binding towards NMBAs was significantly stronger compared to that of **ACh**.

Dialysis experiments were conducted to evaluate the capability of **FOF-SS1-3** to encapsulate **Cis**. Briefly, a solution of **FOF-SS1-3** (10 mg mL^{-1}) and **Cis** (1 mg mL^{-1}) in phosphate buffered saline (PBS, pH 7.4) was kept in a dialysis bag (MWCO 1000), and dialyzed against PBS. A solution of **Cis** alone was used as the control group. The dialysis rate of **Cis** escaping from the dialysis bag was determined by high-performance liquid chromatography (HPLC), and plotted against time. A concentration-absorption standard curve of **Cis** was plotted which represented absolute linearity ($R^2 = 0.9996$, Fig. S25†). As shown in Fig. 3c, while approximately 30% of **Cis** escaped from the dialysis bag containing a solution of **Cis** within one hour, **FOF-SS1-3** reduced the escaping rate to no more than 5%. **FOF-SS3** demonstrated the best retaining ability due to its highest binding strength.

Biocompatibility of FOFs *in vitro*

Cytotoxicity and hemolysis assays were used to verify the biocompatibility of FOFs. The cytotoxicity of **FOF-SS1-3** for L02 and H9C2 cells was evaluated using CCK-8 assay. The results showed that the cells maintain a high survival rate (>85%) even at the highest concentration of **FOF-SS1-3** (512 μg mL^{-1}). There was no noticeable sign of apoptosis, indicating the low
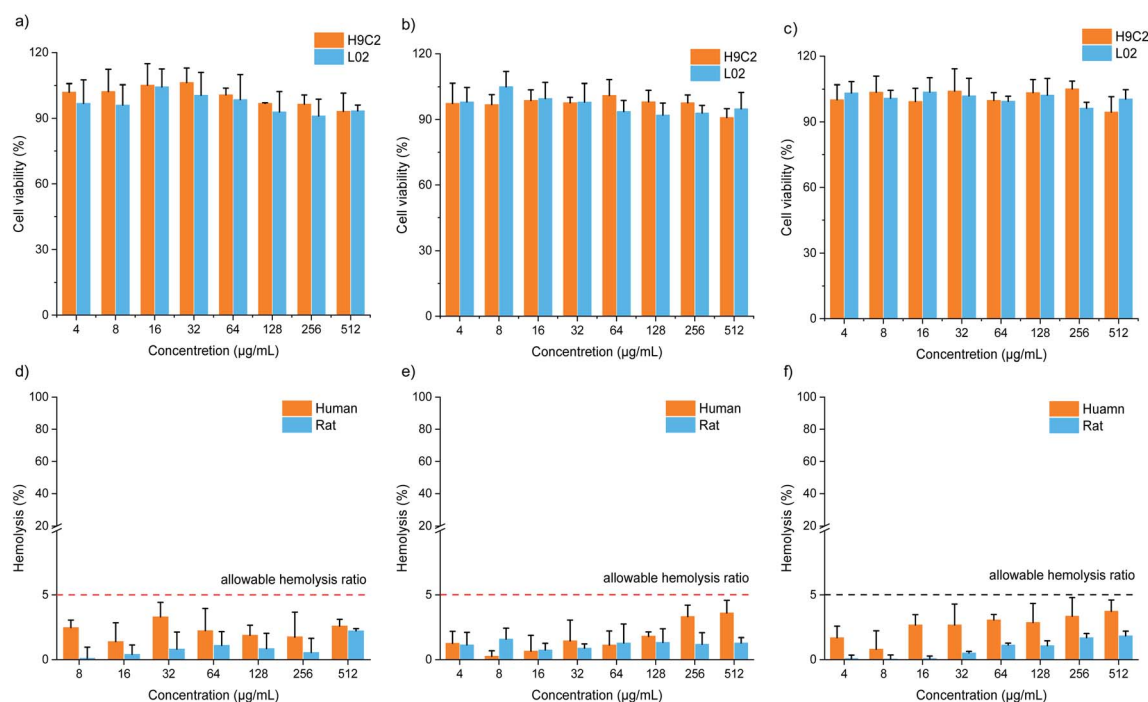

Fig. 4 Cell viability values (%) of H9C2 and L02 cells estimated by CCK-8 *versus* incubation concentrations of (a) **FOF-SS1**, (b) **FOF-SS2**, and (c) **FOF-SS3**. The hemolytic ratio (%) of human and rat erythrocytes *versus* incubation concentrations of (d) **FOF-SS1**, (e) **FOF-SS2**, and (f) **FOF-SS3**.

cytotoxicity (Fig. 4a–c). To carry out the hemolysis assay, healthy erythrocytes were transferred into centrifuge tubes and saline with different concentrations of **FOF-SS1-3**. The absorbance of each sample was recorded at 545 nm using a microplate reader to determine the erythrocyte cell rupture ratio. As shown in Fig. 4d–f, the hemolysis rates for all the three **FOF**s were below 5%, which proved that they did not induce hemolysis.[39]

Experiment for reversal of NMBAs *in vivo*

Lastly, we tested the ability of **FOF-SS1-3** to reverse NMB *in vivo*. For this purpose, rats ($n = 6$) were anesthetized with isoflurane and instrumented with an intravenous line, an arterial line and electrodes to stimulate the femoral nerve. The twitch response of the quadriceps muscle was measured by the acceleration sensor of the Algo TOF-Watch monitor with continuous stimulation at 10 mA current. The monitor was calibrated to ensure a stable response to stimulation, and then switched to TOF mode with continuous stimulation. As the anesthesia started, mechanical ventilation was used to maintain the breath, and **Cis** was administered by intravenous injection (0.6 mg kg^{-1}, two-fold ED90).[18] Thirty seconds later, the quadriceps muscles were completely relaxed (**T1** and TOF to 0). Rats were administrated with placebo (0.5 mL), neostigmine bromide (0.06–0.24 mg kg^{-1}) or **FOF-SS1-3** (40–120 mg kg^{-1}).

As shown in Fig. 5, **FOF-SS1-3** can significantly accelerate the recovery of neuromuscular transmission (TOF to 90%) compared with a placebo and neostigmine (placebo: 774 ± 127 s; neostigmine: 210 ± 19 s; **FOF-SS1**: 202 ± 42 s; **FOF-SS2**: 187 ± 36 s; **FOF-SS3**: 115 ± 17 s). The clinical drug neostigmine could shorten the recovery time of NMB induced by **Cis** compared with a placebo, which was based on the strategy of inhibiting the hydrolysis of acetylcholine.[40] Herein we adopted the strategy of sequestering NMBAs to accelerate the recovery of nerve transmission. **FOF-SS1-3** could shorten the time by 2.8, 3.1 and 5.7-fold compared to the spontaneous recovery time at the maximum dose. **FOF-SS3** showed the highest reversal efficiency, which was consistent with its highest K_a value based on ITC. The recovery time was further shortened than that of neostigmine. Simultaneously, we could observe that with the increasing dosage of FOFs, it showed a significantly improved antagonistic effect against NMB. For **FOF-SS3**, it reached a plateau at 60 mg kg^{-1} while **FOF-SS1-2** may achieve it at a higher dose.

Encouraged by the good performance in reversing **Cis** induced NMB, we further explored the potential application of **FOF-SS3** in reversing NMB induced by **Roc** or **Vec**. **FOF-SS3** significantly accelerated the reversal of NMB induced by **Roc** (placebo: 510 ± 118 s; neostigmine: 362 ± 38 s; **FOF-SS3**: 142 ± 7.5 s) and **Vec** (placebo: 555 ± 112 s; neostigmine: 313 ± 64 s; **FOF-SS3**: 115 ± 19 s). We found that neostigmine can slightly shorten the recovery time while **FOF-SS3** could further shorten the time to a train-of-four ratio of 0.9 by 2.6 and 3.8-fold compared to placebo. **FOF-SS3** could antagonize benzylisoquinolinium and aminosteroid NMBAs, which may act as a broad-spectrum reversal agent, while the commercial drug sugammadex was only used for aminosteroid NMBAs.
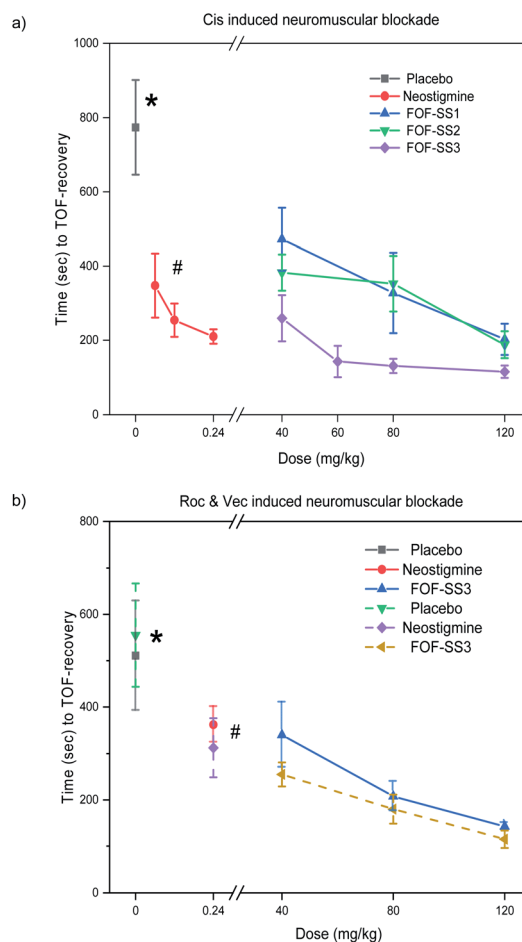

Fig. 5 Time to train-of-four (TOF) ratio of 0.9 recovery from: (a) Cis, (b) Roc (solid line) and Vec (dotted line) induced NMB after administration of FOFS, neostigmine or placebo. **FOF-SS3** accelerated recovery significantly compared with a placebo (*P < 0.0001).

Conclusions

In summary, we constructed three negatively charged and disulfide cross-linked FOFs by oxidative coupling of sulfhydryl groups. FOFs are capable of encapsulating NMBAs due to the synergy between electrostatic and hydrophobic interactions. These FOFs are nontoxic and biocompatible. Animal studies confirm that FOFs are able to efficiently reverse NMB *in vivo*. This study paves the way to explore other clinical applications of supramolecular sequestration by framework materials.

Data availability

Experimental data are available from the authors upon reasonable request.

Author contributions

Y. Wu performed the experiments and wrote the manuscript. Y. Y. Liu, H. K. Liu and S. B. Yu guided the cell cytotoxicity experiment and dialysis experiment. F. Lin, H. Wang, and D. W. Zhang participated in data analysis. W. Zhou and D. Ma

provided mentorship for the *in vivo* experiments. D. Ma and Z. T. Li conceptualized the study and revised the manuscript. All authors were involved in the preparation of the manuscript.

Conflicts of interest

The authors declare no conflict of interests.

Acknowledgements

References

1 C. L. Deng, S. L. Murkli and L. Issacs, *Chem. Soc. Rev.*, 2020, **49**, 7516–7532.
2 S. M. Bromfield, E. Wilde and D. K. Smith, *Chem. Soc. Rev.*, 2013, **42**, 9184–9195.
3 Y. C. Pan, Y. X. Yue, X. Y. Hu, H. B. Li and D. S. Guo, *Adv. Mater.*, 2021, **33**, 2104310.
4 P. T. Bremer, A. Kimishima, J. E. Schlosburg, B. Zhou, K. C. Collins and K. D. Janda, *Angew. Chem., Int. Ed.*, 2016, **55**, 3772–3775.
5 A. Dahan, L. Aarts and T. W. Smith, *Anesthesiology*, 2010, **112**, 226–238.
6 S. Ganapati, S. D. Grabitz, S. Murkli, F. Scheffenbichler, M. I. Rudolph, P. Y. Zavalij, M. Eikermann and L. Isaacs, *ChemBioChem*, 2017, **18**, 1583–1588.
7 Q. Huang, H. Zhao, M. Shui, D. S. Guo and R. Wang, *Chem. Sci.*, 2020, **11**, 9623–9629.
8 T. Mecca, G. M. L. Consoli, C. Geraci, R. L. Spina and F. Cunsolo, *Org. Biomol. Chem.*, 2006, **4**, 3763–3768.
9 U. Hoffmann, M. Grosse-Sundrup, K. Eikermann-Haerter, S. Zaremba, C. Ayata, B. Zhang, D. Ma, L. Isaacs and M. Eikermann, *Anesthesiology*, 2013, **119**, 317–325.
10 D. N. Shurpik, O. A. Mostovaya, D. A. Sevastyanov, O. A. Lenina, A. S. Sapunova, A. D. Voloshina, K. A. Petrov, I. V. Kovyazina, P. J. Cragg and I. I. Stoikov, *Org. Biomol. Chem.*, 2019, **17**, 9951–9959.
11 H. Yin, D. Bardelang and R. Wang, *Trends Chem.*, 2021, **3**, 1–4.
12 K. Wang, D. S. Guo, H. Q. Zhang, D. Li, X. L. Zheng and Y. Liu, *J. Med. Chem.*, 2009, **52**, 6402–6412.
13 H. Chen, J. Y. W. Chan, S. Li, J. J. Liu, I. W. Wyman, S. M. Y. Lee, D. H. Macartney and R. Wang, *RSC Adv.*, 2015, **5**, 63745–63752.
14 Y. M. Zhang, X. Xu, Q. Yu, Y. H. Liu, Y. H. Zhang, L. X. Chen and Y. Liu, *J. Med. Chem.*, 2017, **60**, 3266–3274.
15 A. Bom, M. Bradley, K. Cameron, J. K. Clark, J. Egmond, H. Feilden, E. J. MacLean, A. W. Muir, R. Palin, D. C. Rees and M. Q. Zhang, *Angew. Chem., Int. Ed.*, 2002, **41**, 265–270.
16 J. M. Adam, D. J. Bennett, A. Bom, J. K. Clark, H. Feilden, E. J. Hutchinson, R. Palin, A. Prosser, D. C. Rees, G. M. Rosair, D. Stevenson, G. J. Tarver and M. Q. Zhang, *J. Med. Chem.*, 2002, **45**, 1806–1816.
17 W. T. Nicholson, J. Sprung and C. J. Jankowski, *Pharmacotherapy*, 2007, **27**, 1181–1188.
18 D. Ma, B. Zhang, U. Hoffmann, M. G. Sundrup, M. Eikermann and L. Isaacs, *Angew. Chem., Int. Ed.*, 2012, **51**, 11358–11362.
19 F. Haerter, J. C. P. Simons, U. Foerster, I. M. Duarte, D. Diaz-Gil, S. Ganapati, K. Eikermann-Haerter, C. Ayata, B. Zhang, M. Blobner, L. Isaacs and M. Eikermann, *Anesthesiology*, 2015, **123**, 1337–1349.
20 W. Xue, P. Y. Zavalij and L. Isaacs, *Angew. Chem., Int. Ed.*, 2020, **59**, 13313–13319.
21 X. Zhang, Q. Cheng, L. Li, L. Shangguan, C. Li, S. Li, F. Huang, J. Zhang and R. Wang, *Theranostics*, 2019, **9**, 3107–3121.
22 S. B. Yu, F. Lin, J. Tian, J. Yu, D. W. Zhang and Z. T. Li, *Chem. Soc. Rev.*, 2022, **51**, 434–449.
23 J. Tian, H. Wang, D. W. Zhang, Y. Liu and Z. T. Li, *Nat. Sci. Rev.*, 2017, **4**, 426–436.
24 K. Lu, C. He and W. Lin, *J. Am. Chem. Soc.*, 2014, **136**, 16712–16715.
25 J. Li, C. Zhang, S. Gong, X. Li, M. Yu, C. Qian, H. Qiao and M. Sun, *Acta Biomater.*, 2019, **94**, 435–446.
26 X. He, Y. Yu and Y. Li, *RSC Adv.*, 2018, **8**, 41976–41985.
27 Q. Fang, J. Wang, S. Gu, R. B. Kaspar, Z. Zhuang, J. Zheng, H. Guo, S. Qiu and Y. Yan, *J. Am. Chem. Soc.*, 2015, **137**, 8352–8355.
28 Y. Peng, Y. Huang, Y. Zhu, B. Chen, L. Wang, Z. Lai, Z. Zhang, M. Zhao, C. Tan, N. Yang, F. Shao, Y. Han and H. Zhang, *J. Am. Chem. Soc.*, 2017, **139**, 8698–8704.
29 Y. C. Zhang, P. Y. Zeng, Z. Q. Ma, Z. Y. Xu, Z. K. Wang, B. Guo, F. Yang and Z. T. Li, *Drug Delivery*, 2022, **29**, 128–137.
30 B. Yang, X. D. Zhang, J. Li, J. Tian, Y. P. Wu, F. X. Yu, R. Wang, H. Wang, D. W. Zhang, Y. Liu, L. Zhou and Z. T. Li, *CCS Chem.*, 2019, **1**, 156–165.
31 J. Tian, B. Huang, Z. Cui, P. Wang, S. Chen, G. Yang and W. Zhang, *Acta Biomater.*, 2021, **130**, 447–459.
32 J. L. Lin, Z. K. Wang, Z. Y. Xu, L. Wei, Y. C. Zhang, H. Wang, D. W. Zhang, W. Zhou, Y. B. Zhang, Y. Liu and Z. T. Li, *J. Am. Chem. Soc.*, 2020, **142**, 3577–3582.
33 Z. Y. Xu, H. K. Liu, Y. Wu, Y. C. Zhang, W. Zhou, H. Wang, D. W. Zhang, D. Ma and Z. T. Li, *ACS Appl. Bio. Mater.*, 2021, **4**, 4591–4597.
34 Z. K. Wang, J. L. Lin, Y. C. Zhang, C. W. Yang, Y. K. Zhao, Z. W. Leng, H. Wang, D. W. Zhang, J. Zhu and Z. T. Li, *Mater. Chem. Front.*, 2021, **5**, 869–875.
35 L. Felix, U. Sezer, M. Arndt and M. Mayor, *Eur. J. Org. Chem.*, 2014, **2014**, 6884–6895.
36 D. Liu, Z. Xie, L. Ma and W. Lin, *Inorg. Chem.*, 2010, **49**, 9107–9109.
37 M. Kirihara, Y. Asai, S. Ogawa, T. Noguchi, A. Hatano and Y. Hiraib, *Synthesis*, 2007, **21**, 3286–3289.
38 N. Mistry, A. D. Roberts, G. E. Tranter, P. Francis, I. Barylski, I. M. Ismail, J. K. Nicholson and J. C. Lindon, *Anal. Chem.*, 1999, **71**, 2838–2843.
39 R. Zhao, T. Ma, F. Cui, Y. Tian and G. Zhu, *Adv. Sci.*, 2020, **7**, 2001899.
40 J. Luo, S. Chen, S. Min and L. Peng, *Ther. Clin. Risk Manag.*, 2018, **14**, 2397–2406.